The Determination of Wind Speeds in the Boundary Layer by Monostatic Lidar

E. W. ELORANTA, J. M. KING[1] AND J. A. WEINMAN

Department of Meteorology, University of Wisconsin, Madison 53706

(Manuscript received 10 February 1975, in revised form 14 August 1975)

ABSTRACT

Vertical profiles of the horizontal radial wind component in the lowest kilometer of the atmosphere have been measured remotely with lidar. Wind speed determinations were made by observing the motion of naturally occurring aerosol density inhomogeneities. Lidar wind measurements compare favorably with simultaneous pilot balloon observations of the wind.

1. Introduction

Knowledge of the spatial and temporal variability of wind structure is often required by applied meteorologists. Such activities as aviation takeoffs and landings, prediction of air pollution dispersal, rocket launchings, and boundary layer research can benefit from a real-time remote sensing technique for obtaining wind profiles.

This study demonstrates the feasibility of measuring vertical profiles of the radial component of the horizontal wind by means of a monostatic lidar configured as shown in Fig. 1. Optical backscattering from the atmosphere is strongly dependent on aerosol loading. Aerosols are efficient wind tracers because they respond rapidly to changes in the air velocity. Turbulence, humidity variations, and intermitent aerosol sources provide spatial inhomogeneities in the naturally occurring aerosol content of the boundary layer. These aerosol density inhomogeneities provide a tracer by which radial wind components along the lidar beam can be determined. Lidar data show that density inhomogeneities with horizontal dimensions of ~100 m move consistently with the wind. The lidar data are spatially filtered and cross correlations are computed as a function of time lag to derive the velocities of the density inhomogeneities. It will be shown that wind profiles obtained with lidar compare well with those obtained by concurrent single-theodolite balloon tracking.

Past studies of related techniques include the work by Beneditti-Michelangeli *et al.* (1972) who interferometrically detected the optical Doppler shift of light backscattered from atmospheric aerosols at night. Derr and Little (1970) and Zuev *et al.* (1973) have proposed using cell-correlation methods to track naturally occurring aerosols traveling between spaced lidar beams in order to monitor wind velocities at various altitudes. Also, a passive crossed-beam correlation technique has been described by Krause *et al.* (1970).

[1] Present affiliation: Kirtland A.F.B., N. M. 87117.

2. Observations

Parameters describing the Wisconsin lidar are summarized in Table 1.

For this study the lidar was pointed in the direction of the surface wind and inclined at a 10° elevation

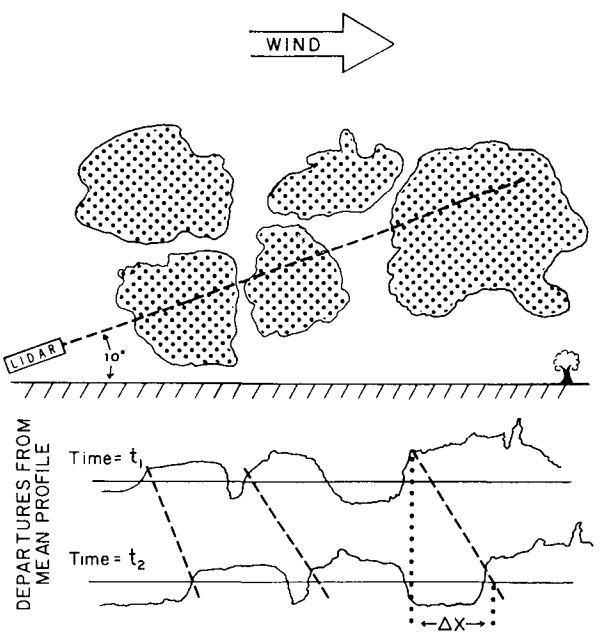

FIG. 1. Basic wind determination scheme. The lidar is aligned with the surface wind direction and elevated by 10°. Aerosol inhomogeneities depicted as shaded areas produce fluctuations in the received lidar return. These variations, shown as departures from the mean lidar profile, are displaced as the aerosols drift with the wind. The radial component of the wind is then $\Delta x/(t_2-t_1)$.

TABLE 1. Parameters of the University of Wisconsin lidar system (1973).

Transmitter	
Operating wavelength	694.3 nm (ruby)
Output energy/pulse	1 J (real-time monitored)
Repetition rate	<0.05 s^{-1}
Pulse duration	20 ns (Pockels Cell Q Switch)
Beam divergence	3 mrad (0.05 m diam telescope)
Receiver	
Telescope	0.20 m diam Newtonian (astronomical quality)
Spectral resolution	2 nm (interference filter)
Detector	RCA C7004K photomultiplier with extended red response multi-alkali cathode
Data logging system	
Amplifier	log: 80 dB range
Storage	1024 8-bit words
Sampling rate	10 words μs^{-1}
Output	real time, scope and paper tape

angle. In a typical observation period a series of 50–200 lidar backscatter profiles were recorded at ~20 s time intervals. The received lidar signals were logarithmically amplified and then digitized at 15 m range intervals with an 8-bit A/D converter. Usable aerosol structure information was obtained for altitudes between 175 and 1300 m above ground level.

Independent measurements of the wind profile were provided by single-theodolite tracking of 0.03 kg pilot balloons. The ascent rate (3.12 m s^{-1}) and corrections due to turbulence in the first 5 min of ascent were calculated for a 0.03 kg balloon with a free lift of 0.139 kg (see Middleton and Spilhaus, 1953). Azimuth and elevation angles for all soundings were read to 0.01° at 30 s intervals using a Warren-Knight Model 84 balloon theodolite and a stopwatch. Balloon velocities were computed to 0.05 m s^{-1} over 30 s intervals with the height taken at the midpoint of the time interval. The velocities were calculated on a non-overlapping basis to obtain maximum velocity detail.

3. Analysis of data

a. The lidar equation

The lidar equation for singly scattered returned power is

$$P_r(x)=\frac{E_0 A c \beta'_{180°}}{8\pi x^2}\exp\left[-2\int_0^x \sigma(x')dx'\right], \quad (1)$$

where:

P_r	received power
E_0	transmitted energy
c	speed of light
x	range, radially outward along the lidar beam
$\beta'_{180°}$	volume backscattering coefficient
A	effective receiver aperture
σ	extinction coefficient.

The received power is normalized to compensate for varying transmitted energy from shot to shot and the return is corrected for the inverse range-squared dependency. Eq. (1) can then be rewritten in the form

$$P(x)=\frac{x^2}{E_0}P_r(x)=K\beta'_{180°}\exp\left[-2\int_0^x \sigma(x')dx'\right], \quad (2)$$

where K is the system constant. $P(x)$, the corrected power returned from range x, is proportional to the backscattering coefficient and to the range-integrated effect of the extinction. A mean corrected lidar return of nine shots at the beginning of the 25 July 1973 lidar run is shown in Fig. 2.

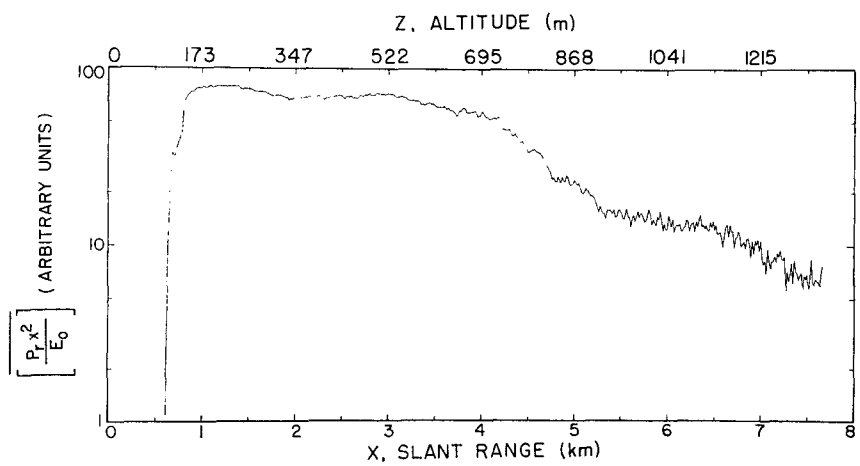

FIG. 2. The mean of nine backscattered lidar returns which are corrected for the inverse range-square dependence and normalized by the transmitted energy [see Eq. (2)]. Data for this profile were obtained on 25 July 1973. Lidar returns are meaningful only for slant ranges beyond the point of full beam overlap which occurred at approximately 1 km.

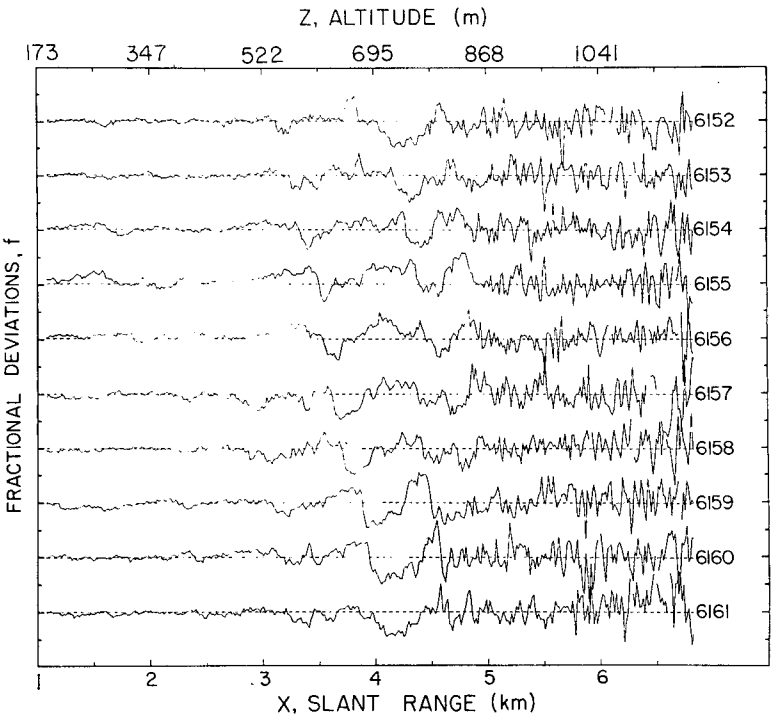

FIG. 3. Lidar deviations calculated from Eq. (3) which were measured on 25 July 1973. The dashed lines represent zero-deviation values for each profile. Numbers at the right-hand side of the graph designate the profile. Profiles were acquired at 20 s intervals.

b. Cross correlation of aerosol density deviations

Wind information in the lidar returns is contained in the motion of aerosol inhomogeneities. The time-varying inhomogeneities are separated from the mean structure of the return by forming fractional deviation profiles $f(x_i,t_n)$ as follows:

$$f(x_i,t_n)=[P(x_i,t_n)-\overline{P(x_i)}]/\overline{P(x_i)}, \qquad (3)$$

where the $P(x_i,t_n)$ are digitized values of the corrected lidar returned power; and

$$\overline{P(x_i)}=\frac{1}{N}\sum_{n=1}^{N} P(x_i,t_n),$$

where x_i is the range at the ith data point, t_n is the time of the nth lidar profile, and N the number of profiles used to obtain the mean profile. Examples of fractional deviation profiles obtained from Eq. (3) are shown in Fig. 3.

The fractional deviation profiles defined by (3) are filtered to suppress both noise produced by non-persistent small eddies and gross features, such as orographic convective plumes, which may not drift with the mean wind. The filter shown below rejects aerosol structure of size less than 60 m and greater than 360 m:

$$F(x_i,t_n)=\sum_{j=i-8}^{i+8} f(x_j,t_n)\exp[-\alpha^2(x_i-x_j)^2]/\sum_{j=i-8}^{i+8}\exp[-\alpha^2(x_i-x_j)^2]-\sum_{j=i-18}^{i+18} f(x_j,t_n)\exp[-\gamma^2(x_i-x_j)^2]/\sum_{j=i-18}^{i+18}\exp[-\gamma^2(x_i-x_j)^2], \qquad (4)$$

where $\alpha=3.3\times10^{-2}$ m^{-2} and $\gamma=5.5\times10^{-3}$ m^{-2}.

The lag cross correlation function $\rho(L, z_1, z_2)$ which is used to determine wind speed in the altitude interval z_1 to z_2 is defined as

$$\rho(L,z_1,z_2)=\frac{1}{\sigma\cdot\sigma_L}\sum_{n=1}^{N-1}\sum_{i=J_1}^{J_2} F(x_i,t_n)\cdot F(x_{i+L},t_{n+1}), \qquad (5)$$

where:

L	lag value
z	altitude
J_i	data point at altitude z_i; $J_i=z_i/(\Delta x \sin\theta)$
N	total number of lidar profiles
Δx	data point separation (15 m)
θ	elevation angle (10°)

and

$$\left.\begin{aligned}\sigma^2&=\sum_{n=1}^{N-1}\sum_{i=J_1}^{J_2}F^2(x_i,t_n)\\ \sigma_L^2&=\sum_{n=2}^{N}\sum_{i=J_1}^{J_2}F^2(x_{i+L},t_{n+1})\end{aligned}\right\}.$$

Eq. (5) yields the lag cross correlation between a series of successive fractional deviation pairs. The correlations are formed over $N-1$ successive pairs to reduce random correlations between noise in the deviation profiles. Examples of $\rho(L,z_1,z_2)$ calculated from the 25 July data are shown in Fig. 4.

Using Eq. (6), the wind velocity component V_r parallel to the lidar beam is determined from the lag value L_m at which $\rho(L,z_1,z_2)$ is maximum, i.e.,

$$V_r=L_m\Delta x/\Delta t, \tag{6}$$

where Δt is the time between laser shots. This velocity is related to the horizontal wind V_h by

$$V_r=V_h\cos\theta\cos\phi, \tag{7}$$

where θ is the elevation angle and ϕ is the difference between the azimuth of the wind vector and the azimuth of the lidar beam. In this study the elevation angle was $\theta=10°$ and the azimuth of the lidar was aligned approximately with the mean wind direction, so that $\cos\theta\approx\cos\phi\approx1$ and $V_h\approx V_r$.

4. Results and conclusions

Only daytime fair-weather measurements were sought in this study. Surface visibilities were 24 km or more.

TABLE 2. Parameters used in wind profile computations.

Date	Lidar observation period (GMT)	N	Δt (s)
25 July	1830–1843	30	26
4 Sept.	1837–1844	20	23
20 Sept.	2009–2020	22	31
29 Oct.	1934–1949	30	31

The method becomes more reliable as the turbidity increases. Lidar wind profiles were computed from observations on four separate days during the summer and fall of 1973 (25 July, 4 and 20 September, 29 October). The lidar profiles were divided into five slant range intervals of 75 data points each, corresponding to altitude intervals of 195 m. In each interval the cross correlation [Eq. (5)] was calculated for lag values, $-20<L\leqslant20$. Other parameters used in these calculations are given in Table 2. Figs. 5–8 show winds obtained from Eq. (6) plotted at the mid-point of each altitude interval. The wind velocity component parallel to the lidar pointing direction as obtained from pilot balloons is also shown in these figures.

It is evident that the wind profiles derived from these lidar measurements are consistent with those derived from the single-theodolite pibal measurements. The pibal measurements may be expected to be in error by ~2 m s^{-1} (Brooks, 1947; Gabriel and Bellucci, 1951).

The reliability of the lidar wind determination is related to the maximum value of the observed cross

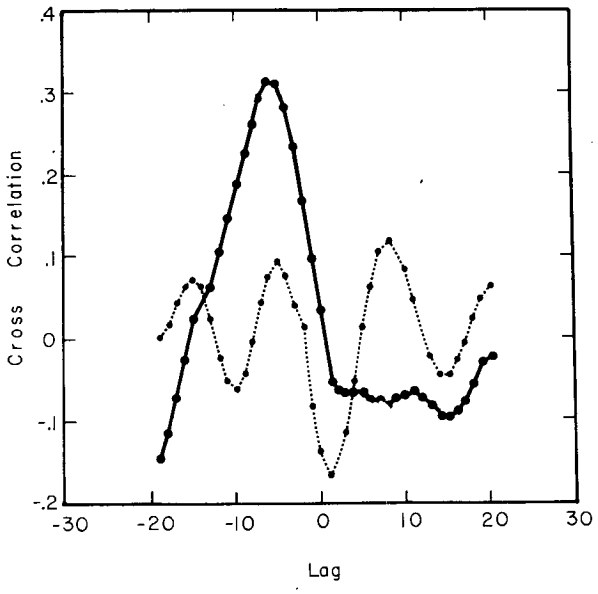

FIG. 4. Cross correlations as a function of lag from Eq. (5) for data obtained on 25 July 1973. The cross-correlation maximum at $L=-7$ for $655\leqslant z\leqslant754$ m (solid line) yields a well-defined wind speed whereas the cross-correlation maximum at $L=-5$ for $951\leqslant z\leqslant1151$ m (dotted line) is not unique.

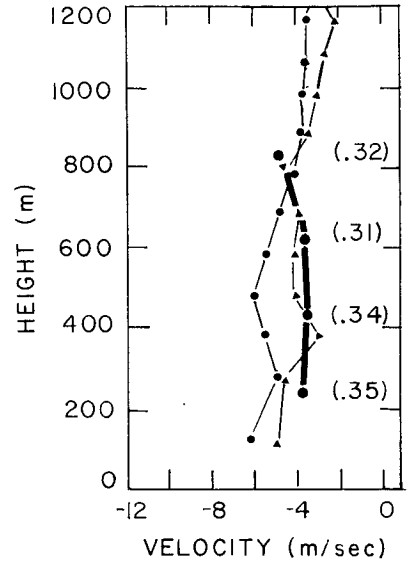

FIG. 5. Radial wind speed component profiles as a function of height from lidar (heavy line) and pilot balloon measurements obtained on 25 July 1973. Pilot balloon launch times were 1745 (▲) and 1924 GMT (●), and the corresponding lidar measurement period is shown in Table 2. Numbers in parentheses are maximum values of the cross-correlation function [Eq. (5)].

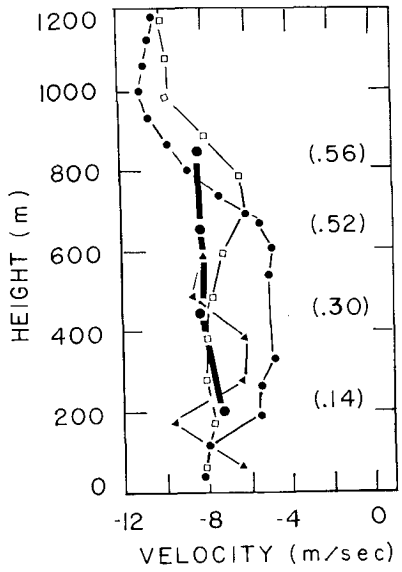

FIG. 6. As in Fig. 5 except for measurements obtained on 4 September 1973 at 1825 (□), 1845 (▲) and 1852 GMT (●).

correlations, $\rho(L,z_1,z_2)$. In practice, noise degrades the lidar signal, the cross beam component of the wind moves aerosol inhomogeneities out of the lidar beam, and the aerosol structure is changed by turbulent mixing processes; these factors produce $\rho(L,z_1,z_2)<1$. The correlations presented in Fig. 4 attain a maximum value of 0.31 in the slab $655\leqslant z\leqslant 754$ m, where Fig. 3 shows that the aerosol structures are persistent and well defined. In the slab $951\leqslant z\leqslant 1151$ m, Fig. 3 shows that $f(x_i,t_n)$ is dominated by shot noise. Here the maximum correlation is reduced to 0.09 and the well-defined peak seen at the lower elevation is replaced by three separate small peaks. At this altitude the wind information is lost in the noise.

Inspection of Figs. 5–8 shows that the cross correlation maxima are greatest at $500\lesssim z\lesssim 900$ m. The spatial extent and persistence of the aerosol inhomogeneities diminish near the surface so that cross-correlation maxima are small near the ground. Since the lidar returns are weak above the mixing layer, statistical shot noise degrades the cross correlation at high altitudes.

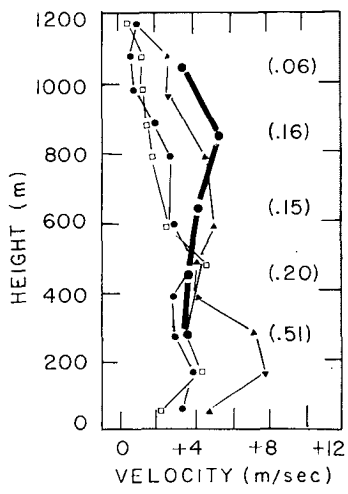

FIG. 7. As in Fig. 5 except for measurements obtained on 20 September 1973 at 2000 (●), 2010 (▲) and 2030 GMT (□).

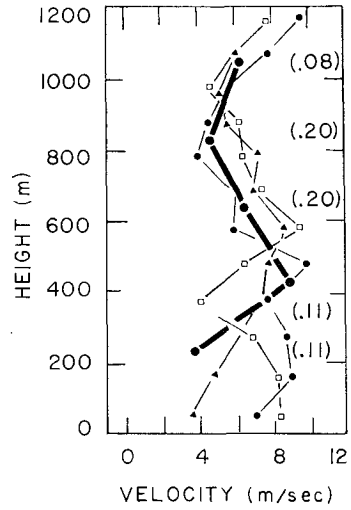

FIG. 8. As in Fig. 5 except for measurements obtained on 29 October 1973 at 1920 (□), 1930 (●) and 1943 GMT (▲).

This study has shown that vertical profiles of the radial wind component in the boundary layer can be remotely measured with a lidar. We are pursuing a more extensive measurement program to determine the range of conditions under which this technique yields useful wind profiles.

Acknowledgments. This study was supported in part by funds provided by U.S.A.R.O.D. Grant 31-124-73-629 and by NSF Grant GA-31562. We thank these agencies for their assistance.

REFERENCES

Benedetti-Michelangeli, G., F. Congeduti and G. Fiocco, 1972: Measurement of aerosol motion and wind velocity in the lower troposphere by Doppler optical radar. *J. Atmos. Sci.*, **29**, 906–910.

Brooks, E. M., 1947: The accuracy and representativeness of the 10,000-foot pibal report. *Bull. Amer. Meteor. Soc.*, **28**, 405–408.

Derr, V. E., and C. G. Little, 1970: A comparison of remote sensing of the clear atmosphere by optical, radio, and acoustic radar techniques. *Appl. Opt.*, **9**, 1982–1983.

Gabriel, J. E., and R. Bellucci, 1951: Time variation of winds aloft. *J. Meteor.*, **8**, 422–423.

Krause, F. R., Ming-Yang Su and E. H. Klugman, 1970: Passive optical detection of meteorological parameters in launch vehicle environments. *Appl. Opt.*, **9**, 1044–1055.

Middleton, W. E. K., and A. F. Spilhaus, 1953: *Meteorological Instruments*. University of Toronto Press, 286 pp.

Zuev, V. E., G. O. Zaddle, V. P. Tarasenko and N. I. Yurga, 1973: Lidar sounding of the atmosphere to estimate static and dynamic characteristics of aerosol inhomogeneities. Presented at Fifth Conf. Laser Radar Studies of the Atmosphere, Williamsburg, Va.